BBE 346 1–11
ARTICLE IN PRESS
BIOCYBERNETICS AND BIOMEDICAL ENGINEERING XXX (2018) XXX–XXX

Available online at www.sciencedirect.com
ScienceDirect
journal homepage: www.elsevier.com/locate/bbe

Original Research Article

Modeling and experimental validation of walking processes

Q1 Raoul R. Nigmatullin[a], Arsenii L. Morozov[a], Jan Awrejcewicz[b,*], Michal Ludwicki[b]

[a] Kazan National Research Technical University, Radioelectronics and Informative-Measurements Technics Department, Karl Marx str., 10, Kazan, Tatarstan 420111, Russian Federation
[b] Lódz University of Technology, Department of Automation, Biomechanics and Mechatronics, 1/15 Stefanowski Street, Lódz 90-924, Poland

ARTICLE INFO

Article history:
Received 27 July 2018
Received in revised form
27 March 2019
Accepted 28 March 2019
Available online xxx

Keywords:
Intermediate model
Motion capture system
Gait
Treadmill
Quasi-reproducible experiment

ABSTRACT

The so-called intermediate model (IM) was applied in the paper to quantitatively describe complex trajectories. Using this model it was possible to find the proper fitting function for describing random trajectories that were recorded during the walking process performed by a volunteer. Experimental data were acquired using a three-dimensional Motion Capture system during normal gait of a healthy person on an automatic treadmill. The major aim of this research was to find if the IM is applicable to fit typical biomechanical measurement data. Motion Capture data collection is very time-consuming and requires a lot of memory, so storing movement trajectories in a parametric form helps to increase the data processing efficiency and mathematical analysis. As a result of the original treatment procedure described in this paper, we obtained a very accurate fit of the measured data. The results of this research can be used to model the movement of mechanical devices and for diagnostic purposes.

1. Introduction and problem formulation

Is it possible to propose a "universal" fitting function for non-stationary quasi-reproducible (QR) experiment? This "unexpected" question sounds irrational to any skeptical researcher. The traditional interaction between theory and experiment is based on a hypothesis and its practical verification. Theorists suggest models based on certain hypotheses and postulates. Experimental researchers validate these hypotheses in the most convincing way, minimizing the impact of any uncontrollable factors and distortions that come from the measured devices or from the external environment. What kind of major improvement/innovation can be made in this conventional scheme?

* Corresponding author at: Lódz University of Technology, Department of Automation, Biomechanics and Mechatronics, 1/15 Stefanowski Street, Lódz 90-924, Poland.
E-mail addresses: renigmat@gmail.com (R.R. Nigmatullin), morozovars@yandex.ru (A.L. Morozov), jan.awrejcewicz@p.lodz.pl (J. Awrejcewicz), michal.ludwicki@p.lodz.pl (M. Ludwicki).
https://doi.org/10.1016/j.bbe.2019.03.005

Let us define the verified principle that can be tested practically in every experiment. If this principle does exist, then from its mathematical formulation a ''universal'' fitting function can be derived which can quantitatively describe any experiment. We will call this principle the Verified Principle of Partial Correlations (VPPC). On this basis, the postulate can be reformulated as follows: subsequent measurements retain their partial correlations (memory) and remain partially correlated as a result of subsequent measurements. To understand this statement more deeply, it is necessary to demonstrate some mathematical formulas given in the next section. In this paper based on the VPPS, we want to consider movement trajectories that can be described in our Intermediate Model and compared with each other.

Trajectories of the movement of living organisms such as mammals are usually very complex so the ''best fit'' model for their description cannot be created. The reason for this are, among others, complex bone and muscle systems, a way to control these systems and muscle redundancy. During muscle cooperation each movement cycle will be slightly different, because there are as many solutions to the task performed as there are combinations that meet a specified target (e.g., [1,2] where the authors analyzed human muscle interactions using experimental and mathematical methods).

Many mathematical models have already been created that describe more or less precisely the dynamics and kinematics of human movement. These investigations concern particular limbs (see, for example, paper [3]) as well as larger parts of the human body (e.g., [4–6]). There are also attempts to develop artificial Central Pattern Generators to describe human locomotion in controlling humanoid robots (e.g., [7,8]). It is also worth mentioning that there are methods using neural networks that generate good quality movement sequences based on machine learning procedures, even for a full human body (e.g. [9]). In this work, we will deal specifically with the human normal gait pattern.

In order to verify biomechanical mathematical models, it is necessary to obtain comparative experimental data. Usually, Motion Capture techniques are used that make it possible to record kinetic and kinematic data of the movement of the entire human body during almost any type of activity. The most important contribution to the development of this branch of knowledge was the professionalization of sports activities.

Experimental data obtained with the use of the Motion Capture technique are associated with high memory consumption, and thus very time-consuming processing. Depending on the required level of accuracy, the registration of the entire human body movement must be described by 37–57 measuring points (called markers) – their trajectories in 3D space. If their number is multiplied by the number of repetitions of a given experiment, its time and the number of volunteers recorded (several dozens for the analysis to be statistically significant), there is a serious problem with storing and even browsing such data. The number of markers and their placement is usually different in every Motion Capture laboratory equipment [10] but it is always large if sufficient accuracy is important. There is, therefore, a justified need to find a way of mathematical description of these specific movement data to facilitate their further processing and analysis.

The method presented in this work allows us to perform function fitting to complex measurement data as long as they are quasi-periodic. This condition is perfectly met by most human normal gait recordings. The purpose of this study was to check whether the presented method applies to fit typical biomechanical measurement data, both the position of motion capture markers and typical joint angle data during the gait cycle.

The paper is organized in the following way. Description of the method is given in Section 2, whereas Section 3 deals with the experimental procedure and data analysis. Section 4 presents the fitting procedure and results obtained, and in the last Section 5 concluding remarks are presented.

2. Description of the method

Because of importance and generality of the proposed intermediate model (IM that is suitable for a wide class of experiments, it is necessary to reproduce the key ideas of this general theory. Some examples of its application are considered in papers [11,12]. It is important to mention that the proposed theory is *self-consistent*. It indicates that we do not use any a priori hypothesis and a ''universal'' fitting function is found from random functions computed only from the real measured data.

By an ''ideal'' experiment (IE) we mean the experiment when the set of subsequent measurements m ($m = 1, 2, \ldots, M$), realized in time T in relation to a given input variable x gives the same response $F(x)$ for any m. In this sense, all measurements performed within IE can be considered as completely correlated. Mathematically, this statement can be written in the following form:

$$F(x + mT) = F(x), \quad m = 0, 1, \ \ldots, \ M-1 \tag{1}$$

It should be mentioned that the input variable x ought to coincide with temporal variable (t), frequency (ω), wavelength (λ), etc. This single-factor experiment implies that other parameters affecting the response function $F(x)$ remain almost constant and unchanged during measurement period T. The solution of this functional equation is well-known and coincides with the segment of the Fourier series $Pr(x \pm T) = Pr(x)$. For discrete data, this segment of the F-series is written as:

$$F(x) \cong Pr(x) = A_0 + \sum_{k=1}^{K>>1} \left[Ac_k \cos\left(2\pi k \frac{x}{T_x}\right) + As_k \sin\left(2\pi k \frac{x}{T_x}\right) \right] \tag{2}$$

Parameter T_x determines a certain mean period with respect to variable x. It is obvious that the requirement of IE (1) cannot be realized in reality and for quasi-reproducible (QR) experiments it is necessary to introduce a more general equation

$$F(x + LT) = \sum_{l=0}^{L-1} \langle a_l(x) \rangle F(x + lT) \tag{3}$$

In this case, it is necessary to find a solution of the functional equation (3). This becomes possible if the set of functions $\langle a_l(x) \rangle$ referred to in (3) is known and satisfies periodic conditions $\langle a_l(x \pm T) \rangle = \langle a_l(x) \rangle$, and in other aspects it may be *arbitrary*. Consider a solution of Eq. (3) when the value of memory parameter L is known. In comparison with this equation, we expect that all subsequent experimental measurements satisfy the following equation

$$F_{L+m}(x) = \sum_{l=0}^{L-1} \langle a_l(x) \rangle F_{l+m}(x), \; m = 0, 1, \ldots, M-1 \tag{4}$$

To obtain functions $\langle a_l(x) \rangle$ ($l = 0, 1, \ldots, L$; $L < M$) we modify the well-known LLSM and presume that the *functional* dispersion assumes the minimal value defined as follows:

$$\sigma(x) = \left[F_{L+m}(x) - \sum_{l=0}^{L-1} \langle a_l(x) \rangle F_{l+m}(x) \right]^2 = \min \tag{5}$$

Taking the derivatives with respect to unidentified functions $\langle a_l(x) \rangle$, we obtain

$$-\frac{\delta\sigma(x)}{\delta\langle a_l(x) \rangle} = \frac{1}{M-L} \sum_{m=0}^{M-L-1} \left[F_{l+m}(x) \left(F_{L+m}(x) - \sum_{s=0}^{L-1} \langle a_s(x) \rangle F_{s+m}(x) \right) \right] = 0 \tag{6}$$

In the next step we perform the smoothing process on all sets of measurement data. It is assumed that the set of functions $\langle a_l(x) \rangle$ ($l = 0, 1, \ldots, L$; $L < M$) is independent of the measurement index m.

The pair of correlation functions

$$K_{L,l} = \frac{1}{M-L} \sum_{m=0}^{M-L-1} F_{L+m}(x) F_{l+m}(x), \; K_{s,l} = \frac{1}{M-L} \sum_{m=0}^{M-L-1} F_{s+m}(x) F_{l+m}(x), \; s, l = 0, 1, \; \ldots, \; L-1 \tag{7}$$

define the system of linear equations that allows us to find functions $\langle a_l(x) \rangle$ from the following equation:

$$\sum_{s=0}^{L-1} K_{s,l}(x) \langle a_s(x) \rangle = K_{L,l}(x), \quad \text{for } l = 0, 1, \; \ldots, \; L-1 \tag{8}$$

The approach presented so far is defined as the *functional* least squares method (FLSM) including the classical LLSM as a *partial* case. Let us come back to the solution of functional equation (4). Now, a solution to Eq. (4) is sought:

$$F_0(x) = [\kappa(x)]^{x/T} Pr(x), \qquad F_m(x) = [\kappa(x)]^{m+x/T} Pr(x) \tag{9}$$

Here, functions $\kappa(x \pm T) = \kappa(x)$, $Pr(x \pm T) = Pr(x)$ are periodic according to conditions $\langle a_l(x \pm T) \rangle = \langle a_l(x) \rangle$, so like in formula (2) they can be described by the fragment of the Fourier series in the following way:

$$\Phi(x) = A_0 + \sum_{k=1}^{K>>1} \left[Ac_k \cos\left(2\pi k \frac{x}{T}\right) + As_k \sin\left(2\pi k \frac{x}{T}\right) \right] \tag{10}$$

Naturally, the decomposition coefficients Ac_k, As_k ($k = 1, 2, \ldots, K$) in (10) depend on the type of the selected function $\Phi(x)$. Substituting the trial solutions (9) into (4), the equation describing unknown functions $\kappa(x)$ is derived:

$$[\kappa(x)]^L - \sum_{l=0}^{L-1} \langle a_l(x) \rangle [\kappa(x)]^l = 0 \tag{11}$$

Assuming that "roots" $\kappa_q(x)$, $q = 1, 2, \ldots, L$ (10) are given by Eq. (11), the general solution $F_m(x)$ can be written as follows:

$$F_0(x) = \sum_{q=1}^{L} [\kappa_q(x)]^{x/T} Pr_q(x), \qquad F_m(x) = \sum_{q=1}^{L} [\kappa_q(x)]^{m+(x/T)} Pr_q(x), \; m = 0, 1, \ldots, M-1 \tag{12}$$

The set of periodic functions $Pr_q(x)$ should correspond to the number of functions described by Eq. (11). Any additional comments and descriptions related to (12) can be found in [11,12].

For further purposes, it will be necessary to use the fitting function for $L = 2$. This function contains the minimum number of fitting parameters and may be suitable for describing movement trajectories. This case will be used for the fitting process in the next section. For $L = 2$ we find

$$F_{2+m}(x) = \langle a_1(x) \rangle F_{1+m} + \langle a_0(x) \rangle F_m, \; m = 0, 1, \ldots, M-1. \tag{13}$$

Eq. (8) for this case takes the following form

$$\begin{aligned} K_{00}(x)\langle a_0(x) \rangle + K_{10}(x)\langle a_1(x) \rangle &= K_{20}(x) \\ K_{10}(x)\langle a_0(x) \rangle + K_{11}(x)\langle a_1(x) \rangle &= K_{21}(x) \end{aligned} \tag{14}$$

The solution of Eq. (13) can be written as

$$F_0(x) = [\kappa_1(x)]^{x/T} Pr_1(x) + [\kappa_2(x)]^{x/T} Pr_2(x), \quad \kappa_{1,2}(x) = \frac{\langle a_1(x) \rangle}{2} \pm \sqrt{\left(\frac{\langle a_1(x) \rangle}{2}\right)^2 + \langle a_0(x) \rangle}. \tag{15}$$

The desired function for the fitting purposes can be presented in the following final form

$$\begin{aligned} & y(x) \cong F(x; K, T_x) = A_0 E_0^{(1)}(x) + \sum_{k=1}^{K} \left(Ac_k^{(1)} Ec_k^{(1)}(x) + As_k^{(1)} Es_k^{(1)} \right) + \sum_{k=1}^{K} \left(Ac_k^{(2)} Ec_k^{(2)}(x) + As_k^{(2)} Es_k^{(2)} \right), \\ & E_0(x) = \left([\kappa_1(x)]^{x/T_x} + Re[\kappa_2(x)]^{x/T_x} \right), \\ & Ec_k^{(1)} = \left([\kappa_1(x)]^{x/T_x} \right) \cdot \cos\left(2\pi k \frac{x}{T_x}\right), \qquad Es_k^{(1)} = \left([\kappa_1(x)]^{x/T_x} \right) \cdot \sin\left(2\pi k \frac{x}{T_x}\right), \\ & Ec_k^{(2)} = Re\left([\kappa_2(x)]^{x/T_x} \right) \cdot \cos\left(2\pi k \frac{x}{T_x}\right), \qquad Es_k^{(2)} = Re\left([\kappa_2(x)]^{x/T_x} \right) \cdot \sin\left(2\pi k \frac{x}{T_x}\right). \end{aligned} \tag{16}$$

Here, the known functions $\kappa_{1,2}(x)$ should be related to reduced values of the smoothened roots. Functions $E_0(x)$, $Ec_k^{(2)}(x)$, $Es_k^{(2)}(x)$ include the possibility that root $\kappa_2(x)$ can be *negative*. Function $F(x; K, T_x)$ contains only two nonlinear fitting parameters. They can be calculated from the minimization of the relative error surface

$$\min\left[RelError\left(\frac{stdev(y(x)-F(x;K,T_x))}{mean(|y(x)|)}\right)\times 100\%\right] \tag{17}$$

that is given by (K, T_x). Usually, the mean period T_x is not known and lies in the interval ($0.5\,T_{in} < T < 2\,T_{in}$), $T_{in} = (x_1-x_0)\cdot$ length(x). The minimum value of final mode K results from the condition that the level of the relative error should be inside the acceptable range (1%–10%). After the process of minimizing the value (17), the desired amplitudes $A_0, Ac_k^{(1,2)}(x), As_k^{(1,2)}(x)$ are found using the LLSM formulas (16).

3. Experimental details and data handling procedure

A three-dimensional Motion Capture system was used to record human movement during normal walking. Our laboratory is equipped with an OptiTrack system (NaturalPoint Inc., Corvallis, OR, USA) consisting of 6 Flex 13 cameras (120 Hz, 850 nm IR strobe LEDs) recording the position of passive and active markers (in infrared light) attached to the body of the subject. In the present research, 37 reflective (passive) markers were placed according to the standard protocol suggested by the systems manufacturer (Baseline Markerset). The OZ axis indicated the direction of walking, the OX axis was transversal to the walking direction, and the OY axis was longitudinal to the direction of gravity force.

The authors of this manuscript declare that the research was organized according to the Helsinki regulations and the participant was a volunteer who was informed in detail about the aim of the research and examination protocol, he also accepted and signed a written consent (conscious agreement). A volunteer (24-year old male, 72.2 kg, 177.5 cm tall) was a student of the Lodz University of Technology and was found by the university announcement. He did not declare any kind of cardiovascular or pulmonary problems, or problems with locomotion system and postural stability. After attaching the markers, the volunteer was asked to stand upright in order to calibrate the system and then after a brief warm-up, he made a 10-min walk on an automatic treadmill with a normal walking speed of about 4 km/h (see Fig. 1). The volunteer gave written informed consent before participating in the experiment.

The obtained data were filtered and post-processed according to standard biomechanical measurement procedures [13,14] and suggestions from the OptiTrack Documentation. Raw measurement data were first processed to find all marker tracking errors (including unlabeled markers, swapped markers and marker occlusion). This process was semi-automatic and needed special attention. After these rectifications, each marker trajectory signal was filtered to eliminate the frequencies not present in human gait. A low-pass Butterworth 4th order filter with a cut-off frequency of 10 Hz was used. In the next step, detection of repeating gait phases was carried out (see Figs. 2 and 3). From the 10-min recording, 510 steps were extracted. In order to meet the requirements of the presented function fitting algorithm, additional cubic spline interpolation was performed to multiply the number of measurement points by 5 to about 650 data points. As a reference marker for determining the successive gait steps (phases), the one placed on the left ankle of the subject was used (labeled ''LAnkleOut'', according to the OptiTrack Baseline protocol placed on the lateral end of the *malleolus* bone). The above data processing procedure was implemented in the SciLab package (open-source MATLAB alternative). The whole processing procedure is presented in Fig. 4.

Trajectories of the left ankle marker were also used to carry out the desired fitting procedure within the intermediate model. The *basic* problem was to find the accurate fit of the averaged $X(t)$, $Y(t)$ and $Z(t)$ trajectories within the intermediate model when the proper mechanical model was *absent*. As an example of typical biomechanical data analysis, also hip, knee and ankle joint angles were processed. We demonstrate and

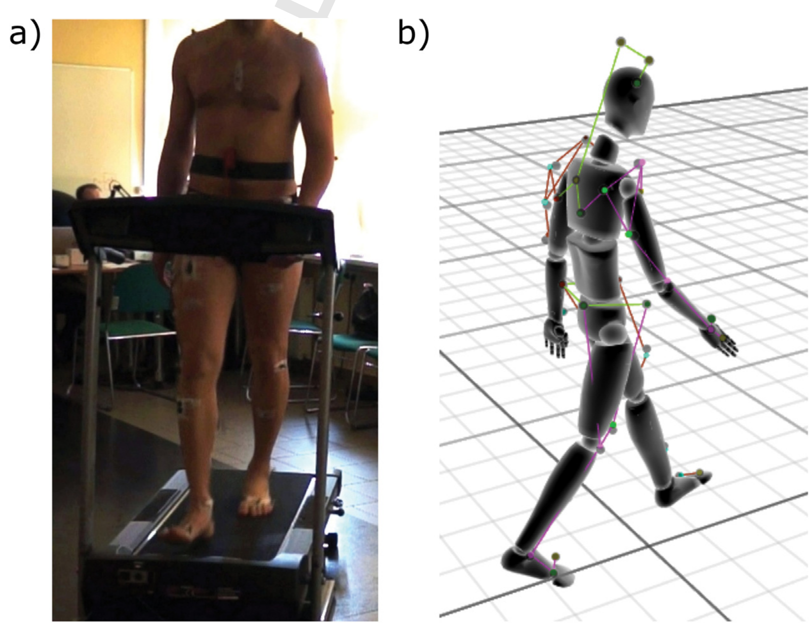

Fig. 1 – (a) Photo of the volunteer equipped with reflective markers and EMG electrodes during normal gait on the treadmill; (b) Motion Capture 3D body reconstruction using 37 reflective markers.

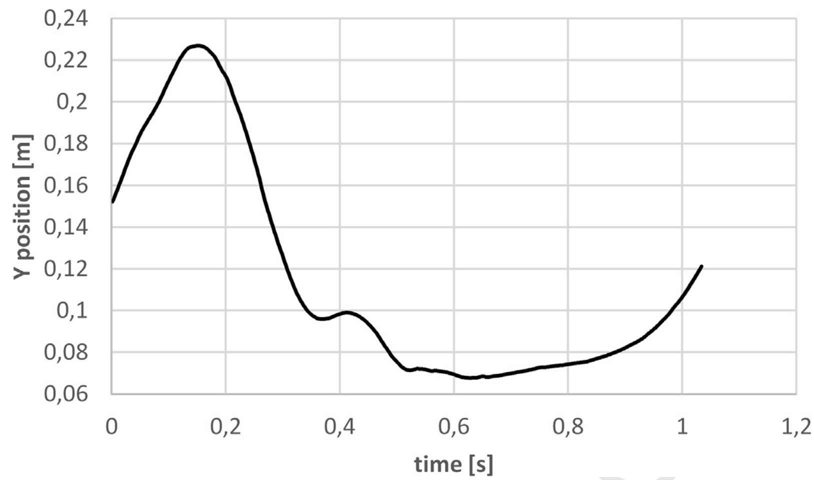

Fig. 2 – Vertical position of the left leg ankle marker during one step in the OY axis direction.

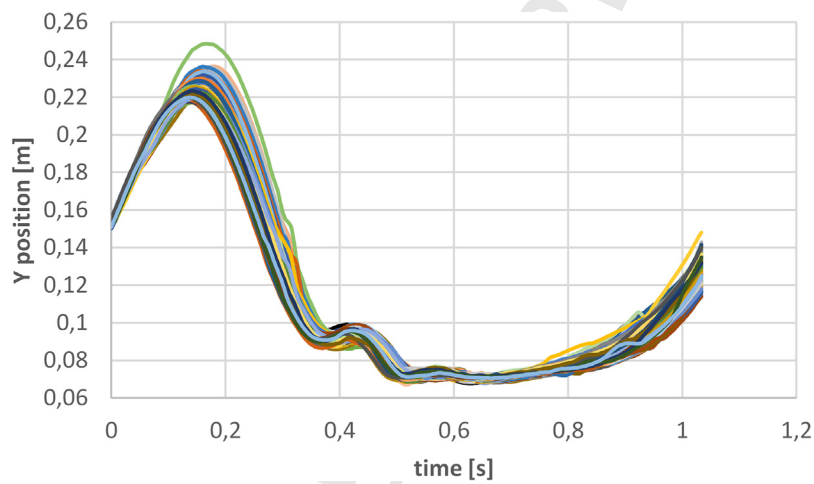

Fig. 3 – Vertical position of the left leg ankle marker after extracting 200 steps realized along the OY axis.

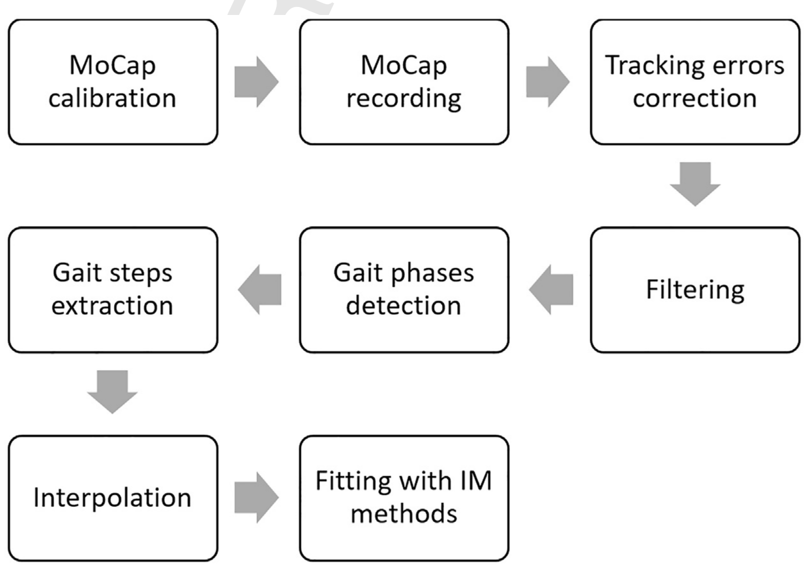

Fig. 4 – Measurement process and data handling.

explain in detail the treatment procedure for trajectories corresponding to the OX axis. Other trajectories along the OY and OZ axes and biomechanical angles data were treated in a similar manner.

4. Fitting procedure and results

In order to obtain the desired fit we divided the whole procedure into the following steps.

4.1. *The clusterization procedure*

Consider the definition of slopes with respect to the mean measurement

$$Sl_m = slope(\langle y\rangle, y_m) \equiv \frac{(y_m \cdot \langle y\rangle)}{(\langle y\rangle \cdot \langle y\rangle)},$$
$$\langle y\rangle = \left(\frac{1}{M}\right)\sum_{m=0}^{M-1} y_m, \quad (A \cdot B) = \sum_{j=1}^{N} A_j B_j. \tag{18}$$

The parenthesis determines the scalar product between two functions including $j = 1, 2, \ldots, N$ measured data points. It is *assumed* here that the initial measurements $y_m(x)$, for $m = 0, 1, \ldots, M-1$, coincide approximately with the functions $F_m(x)$ $(y_m(x) \cong F_m(x))$ appearing in equations (16). If the plot Sl_m is constructed with respect to a subsequent measurement m and then all measurements are rearranged in the descending order $SL_0 > SL_1 > \ldots > SL_{M-1}$, then all performed measurements can be divided into three groups. The first "up" group has slopes located in the first interval $(1 + \Delta, SL_0)$; the mean group (denoted by "mn") has slopes in the range $(1 - \Delta, 1 + \Delta)$; the last "down" group (denoted by "dn") with slopes from $(1 - \Delta, SL_{M-1})$. The value Δ is chosen separately for each set of quasi-reproducible measurements. This procedure is explained in Fig. 5(a–c).

The bell-like curve (BLC) (which can be fitted with the help of four fitting parameters α, β, A, B) is derived after the elimination of the corresponding mean value and the subsequent integration can be described by the beta-function

$$Bd(m; \alpha, \beta, A, B) = A(m)^{\alpha}(M-1-m)^{\beta} + B \tag{19}$$

reflecting the quality of the realized measurements. Quantitatively, all three cases can be characterized by the ratio

$$Rt = \left(\frac{Nmn}{Nup + Ndn + Nmn}\right) \times 100\% = \left(\frac{Nmn}{M}\right) \times 100\% \tag{20}$$

In this case Nup, Ndn and Nmn determine the number of measurements that form the initial "up", final "dn" and middle "mn" part of the beta-distribution, respectively.

In the last expression (20), M determines the total number of corresponding measurements. Based on the Rt ratio it is possible to find three classes of measurements: "good" when $60\% < Rt < 100\%$, "acceptable" when $30\% < Rt < 60\%$, and "bad" when $0 < Rt < 30\%$. This analysis is shown in Figs. 5

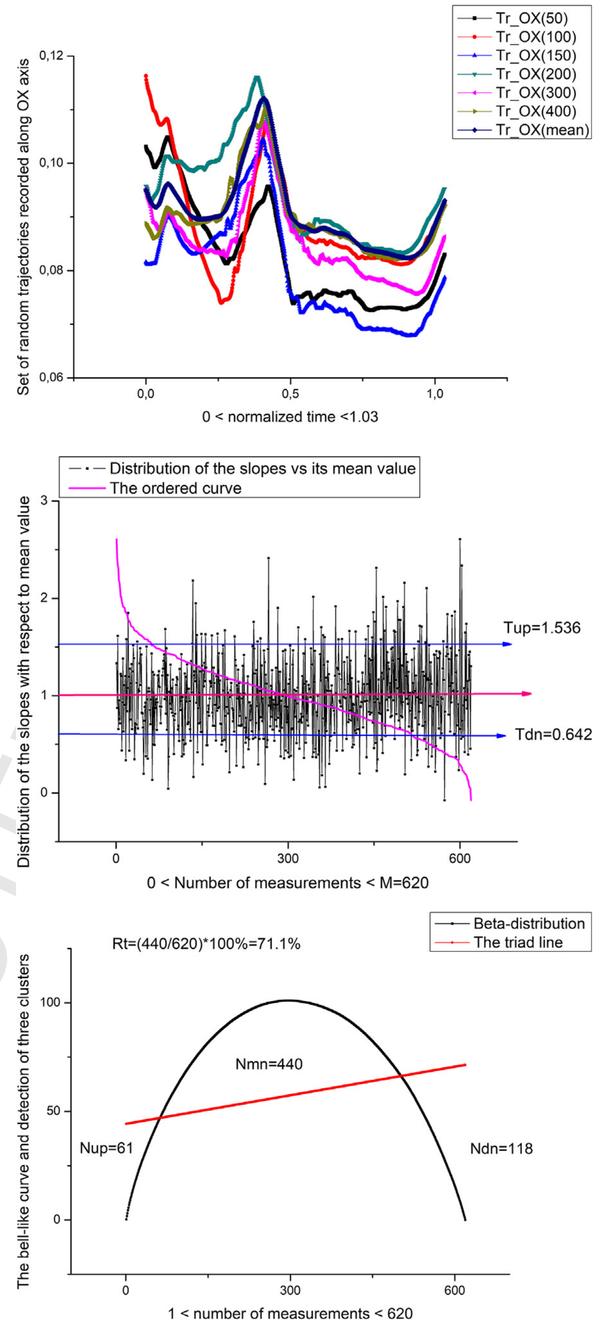

Fig. 5 – (a) The randomly taken trajectories recorded along the OX axis. (b) The distribution of the slopes for OX-trajectory calculated according to Eq. (18). The cyan line corresponds to the ordered measurements. Two blue lines demonstrate the division of all measurements on three clusters in accordance with the 3-sigma criterion explained in the text. (c) After integration of the SRA depicted in the previous figure (cyan line) we obtain a bell-like curve. The red line demonstrates the selection of all measurements on three independent groups (clusters). After averaging all trajectories, only three averaged trajectories are obtained according to Eq. (21). The quality of the realized measurements calculated using Eq. (20) equals Rt = 71.1%.

Please cite this article in press as: Nigmatullin RR, et al. Modeling and experimental validation of walking processes. Biocybern Biomed Eng (2019), https://doi.org/10.1016/j.bbe.2019.03.005

(b and c). Therefore, after the clusterization process instead of Eq. (12) we have approximately

$$
\begin{aligned}
&F_2(x) = \langle a_1(x)\rangle F_1(x) + \langle a_0(x)\rangle F_0(x),\\
&F_2(x) \equiv Yup(x) = \frac{1}{Nup}\sum_{m=0}^{Nup-1} y_m^{(up)}(x), \quad 1+\Delta < Sl_m < SL_0,\\
&F_1(x) \equiv Ydn(x) = \frac{1}{Ndn}\sum_{m=0}^{Ndn-1} y_m^{(dn)}(x), \quad SL_M < Sl_m < 1-\Delta,\\
&F_0(x) \equiv Ymn(x) = \frac{1}{Nmn}\sum_{m=0}^{Nmn-1} y_m^{(mn)}(x), \quad 1-\Delta < Sl_m < 1+\Delta
\end{aligned}
\tag{21}
$$

Here, the SL_m function determines slopes placed in the descending order and the parameter Δ associated with the value of the confidence interval is selected *separately* for each specific set of measurement data. Results of the separation procedure using expression (21) are shown in Fig. 6.

4.2. *The calculation of roots (15)*

The second important stage is related to the calculation of roots according to expression (15). They enter the final fitting function (16) and are shown in Fig. 7.

4.3. *The final fit of the function (16)*

The functions entering the triad are strongly correlated. Therefore, it is instructive to realize the fit only for the Ymn (t) function which is shown in Fig. 8. Some additional parameters are collected in Table 1. The calculated amplitudes $Ac_k^{(1,2)}$, $As_k^{(1,2)}$ are shown in Fig. 9.

In the same way, we treated the trajectories corresponding to the OY and OZ axes. Their final fit is shown in Fig. 10(a and b) along with the desired amplitudes for the OY and OZ trajectories, respectively. Fig. 11(a and b) correspond to the OZ trajectory.

Fitting results for biomechanical angles data are presented in Fig. 12. Other fitting parameters are listed in Table 1. The complete fitting procedure takes about 1–2 min per data file using the code written in MathCad 15, after about 2 min of processing the raw motion capture data in SciLab (see Fig. 4).

5. Discussion and conclusions

In most biomechanical processes, including human body movements, the set of experiments carried out cannot be perfectly repeated each time. This means that even if we use components of the movement of one person, the measurement suffers from the presence of "uncontrollable factors" that would be of interest to the conducted research, but not always. The latter drawback is also associated with the frequently used commercial software applied by biomechanics researchers based on raw marker data, when sometimes averaged or fitted data would be good enough. A good example of this would be to look for a trajectory controlling the movement of a human exoskeleton or other type of equipment that should reproduce human movement. In this case, averaged trajectories from the series of recordings or fitted by our method are sufficient. In the latter case, to obtain validated data, it is necessary to repeat the experiment several times and in a sense to average the digital data to get "reliable" data. Our approach is validated by other experimentally obtained data proving its universality and including the field of biomechanics. This approach has been recently approved by a study of a single heartbeat, showing its nontrivial application to demonstrate its effectiveness in quantitative modeling of ECG data within the proposed theory [12]. In addition, there are other examples showing powerful feature of the proposed approach based on the Prony series including the experimental data associated with typical working conditions of the injection system in a common rail diesel engine [11]. This

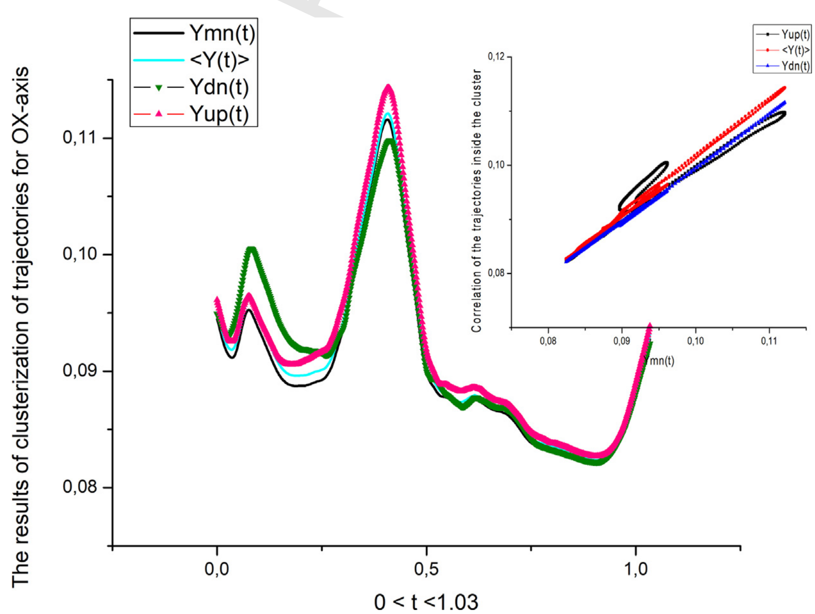

Fig. 6 – The calculated triad of the averaged trajectories for the OX axis. The small figure above shows the strong correlations inside the triad.

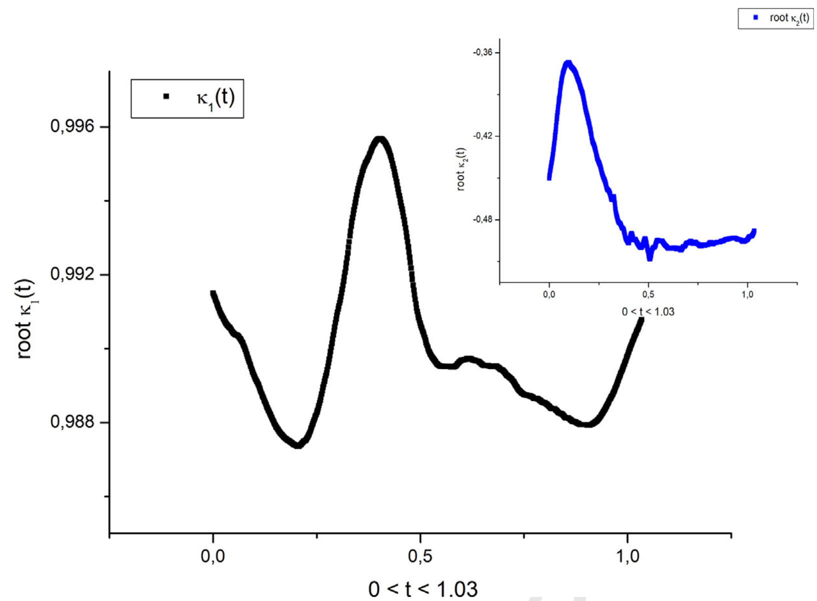

Fig. 7 – The distribution of the roots that enter the final fitting function (16) and are calculated in the frame of the functional least squares method according to Eq. (15).

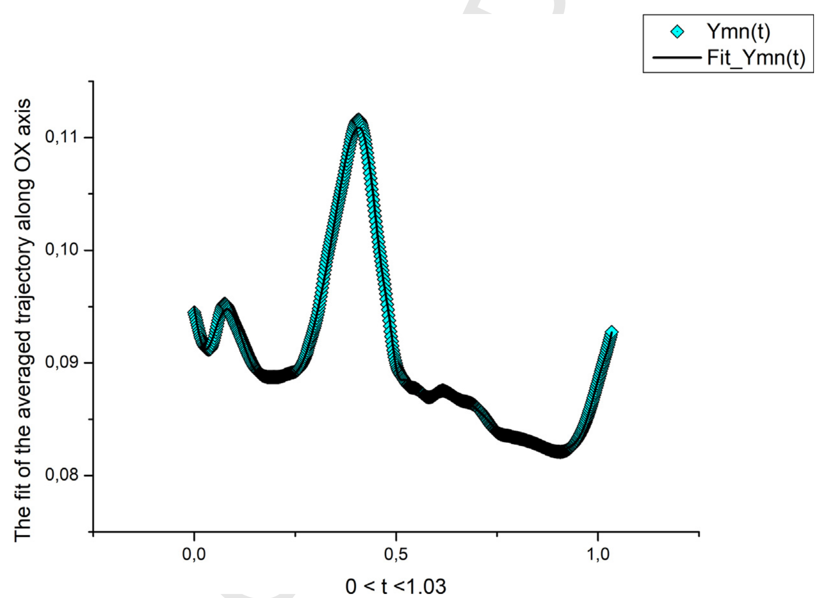

Fig. 8 – The fit of the *Ymn(t)* function corresponding to trajectory along the OX axis. The values of the relative error together with other parameters are listed in Table 1.

Table 1 – Additional parameters that enter to the fitting function (16).

Axes	True value of the period (Ttr)	Range (κ_1)	Range (κ_2)	A_0	Range (Atot)	RelErr (%)	Final mode K
OX	0.70395	0.99562	0.50452	0.11286	0.41876	0.27021	6
OY	0.92134	1.01	0.54473	0.08609	0.31767	0.19829	6
OZ	0.92134	1.002	0.36216	0.46306	0.96584	0.0678	6
Hip	77.1309	1.25	0.41	0.9161	29.7164	1.17939	4
Knee	77.1309	1.19	0.75	20.8911	118.59	0.418289	6
Ankle	77.1309	1.35	0.62	2.3519	88.2102	1.87778	10

The operator "Range" is defined by conventional relationship Range(f) = Max(f) – Min(f). The column 6 determines the total range for all amplitudes that enter in (16). The 7th column determines the value of the fitting error that fit (16) to the averaged values of the trajectories *Ymn* (*t*).

Please cite this article in press as: Nigmatullin RR, et al. Modeling and experimental validation of walking processes. Biocybern Biomed Eng (2019), https://doi.org/10.1016/j.bbe.2019.03.005

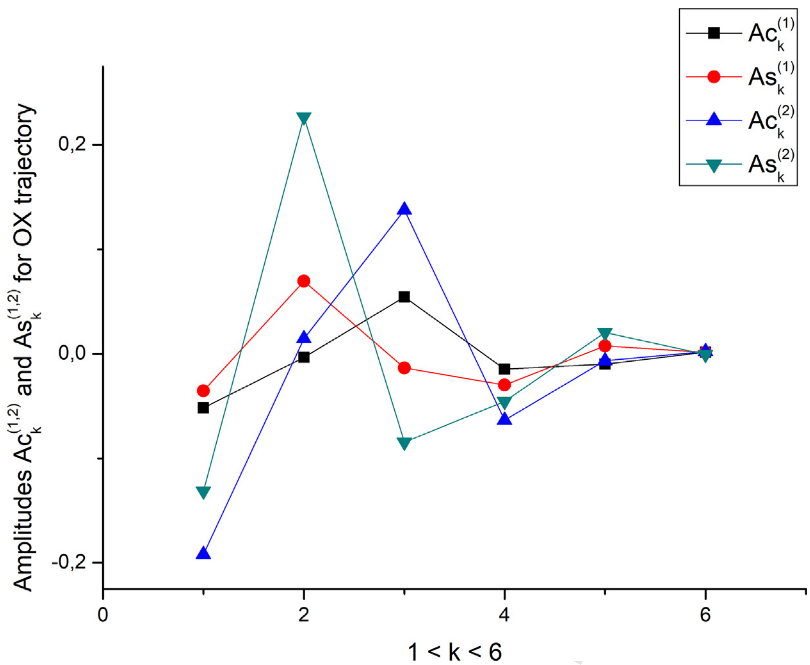

Fig. 9 – The distribution of the $Ac_k^{(1,2)}$, $As_k^{(1,2)}$ amplitudes that enter the fitting function (16) corresponding to the trajectory along the OX axis.

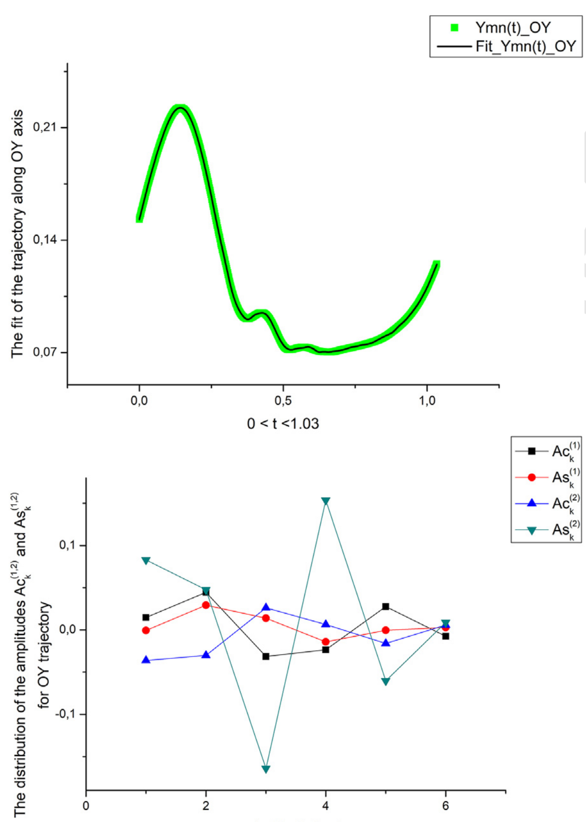

Fig. 10 – (a)The fit of the *Ymn(t)* function corresponding to the trajectory along the OY axis. The values of the relative error together with other parameters are given in Table 1. (b) The distribution of the $Ac_k^{(1,2)}$, $As_k^{(1,2)}$ amplitudes that enter the fitting function (16) corresponding to the trajectory along the OY axis.

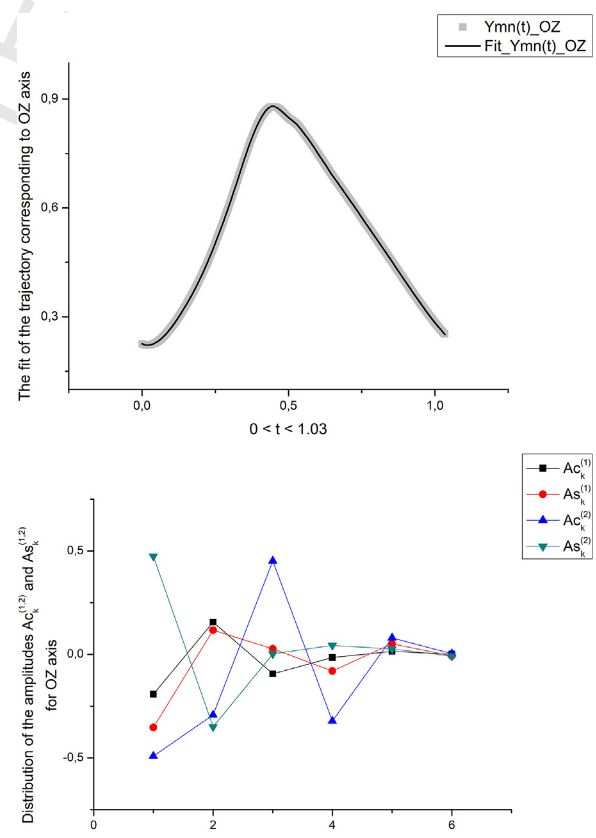

Fig. 11 – (a)The fit of the *Ymn(t)* function corresponding to the trajectory along the OZ axis. The values of the relative error together with other parameters are given in Table 1. (b) The distribution of the amplitudes $Ac_k^{(1,2)}$, $As_k^{(1,2)}$ that enter the fitting function (16) corresponding to the trajectory along the OZ axis.

Please cite this article in press as: Nigmatullin RR, et al. Modeling and experimental validation of walking processes. Biocybern Biomed Eng (2019), https://doi.org/10.1016/j.bbe.2019.03.005

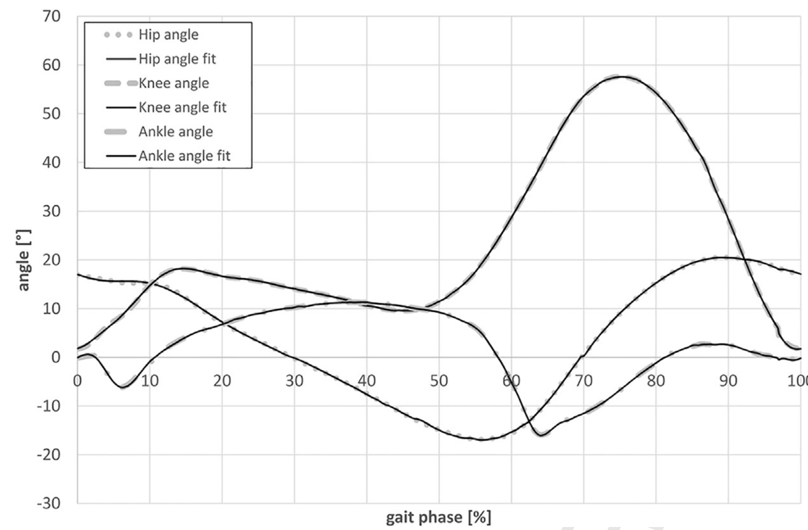

Fig. 12 – The fit of the *Ymn*(*t*) function corresponding to hip, knee and ankle joint angles along medio-lateral direction (OX axis). The value of the relative error together with other parameters are given in Table 1.

means that our approach is validated even for more complex cases and even for instabilities occurring in the measurement process.

It should be emphasized that our theoretical background allows us to describe the experiment associated with quasi-reproducible data reflecting self-similar properties of a wide class of complex systems including those from the field of biomechanics. In addition, the problem is reduced to a set of fitting parameters belonging to the segment of the Prony series. Another advantage is that the analytically derived "best fit" model allows for its employment in other approaches aimed at describing many dynamical phenomena of the human body segments based on ordinary non-linear differential equations. For example, it may play an important role in the adaptation of a control system while carrying out the human postural balance. A robust control strategy including the role of knee, ankle and hip joints based on the analytically developed "best fit" model ensures low numerical costs of simulation of the functioning of these joints. It also minimizes the efforts of the central nervous system to stabilize the body mass center in the presence of small disturbances in the body balance [15].

As presented in previous sections, the fitting procedure consists of a number of processing steps that lead to an equation which represents (fits) the repetitive raw input data.

The mean time of total processing, from raw motion capture data file to a fitting function was about 3–5 min per data file. This is a relatively long time for data processing but it can be shortened. The reconstruction process takes about 1 min to obtain raw data with the original frequency from the fitting function. The most time-consuming point is the search of the minimum value of the relative error surface – expression (17). The authors see the possibility of shortening the calculation time (fitting and reconstruction) after optimizing the code and transferring it from SciLab and MathCad to the MATLAB environment.

The calculated percentage ratio (Eq. (20) and Fig. 5(a–c)) is a good predictor of the quality of the measurement process in terms of biomechanics and stability of the analyzed movement. In this case, we define stability as the ratio of repeatability of the movement. The activity of walking on the treadmill is characterized by constant velocity and constant external conditions such as no obstacles on the walking surface and a flat surface that provides secure support for every step. Under such conditions, any deviation from the average trajectory of movement means certain instability of this movement.

The presented results show that both the data of the 3D marker position and of the three joint angles (hip, knee and ankle), typical for biomechanical analysis, can be parameterized using the described fitting method, with a satisfactory quality of about 1% of the mean error (see Table 1).

It has been shown that IM can be used to store a representative sample of complex biomechanical movement trajectories (or its larger part) in a parametric form, instead of raw measurement data (see Eq. (16) and Figs. 8, 10a and 11a). This important peculiarity will save space for stored data and speed up their subsequent analysis, processing and browsing, after significant optimization of algorithms.

Finally, it is also worth noting that the proposed calculation scheme has a wide range of applications and can be used to parameterize *any* complex trajectory in 3D space after preliminary filtering.

Conflicts of interest

None declared.

Acknowledgment

This work has been supported by the National Science Centre Q3 of Poland under the grant OPUS 9 No. 2015/17/B/ST8/1700.

Please cite this article in press as: Nigmatullin RR, et al. Modeling and experimental validation of walking processes. Biocybern Biomed Eng (2019), https://doi.org/10.1016/j.bbe.2019.03.005

REFERENCES

[1] Gribble PL, Ostry DJ. Compensation for interaction torques during single- and multijoint limb movement. J Neurophysiol 1999;82:2310–26. http://dx.doi.org/10.1152/jn.1999.82.5.2310

[2] Zagrodny B, Ludwicki M, Wojnicz W, Mrozowski J, Awrejcewicz J. Cooperation of mono- and bi-articular muscles: human lower limb. J Musculoskelet Neuronal Interact 2018;18:176–82.

[3] Flash T, Meirovitch Y, Barliya A. Models of human movement: trajectory planning and inverse kinematics studies. Robot Auton Syst 2013;61:330–9. http://dx.doi.org/10.1016/j.robot.2012.09.020

[4] Vimieiro C, Andrada E, Witte H, Pinotti M. A computational model for dynamic analysis of the human gait. Comput Methods Biomech Biomed Eng 2015;18:799–804. http://dx.doi.org/10.1080/10255842.2013.848859

[5] Moreira P, Lugrís U, Cuadrado J, Flores P. Biomechanical models for human gait analyses using inverse dynamics formulation. 5° Congresso Nacional de Biomecânica. Sociedade Portuguesa de Biomecânica; 2013. p. 1–6.

[6] Xiao T, Fu Y-F. Biomechanical modeling of human body movement. J Biom Biostat 2016;7:1–4. http://dx.doi.org/10.4172/2155-6180.1000309

[7] Mondal S, Nandt A, Chakraborty P, Nand GC. A central pattern generator based nonlinear controller to simulate biped locomotion with a stable human gait oscillation. Int J Robot Autom 2011;2:93–106.

[8] Grzelczyk D, Szymanowska O, Awrejcewicz J. Gait pattern generator for control of a lower limb exoskeleton. Vib Phys Syst 2018;29. 2018007:1–10.

[9] Lin X, Amer MR. Human motion modeling using DVGANs; 2018;10652, arXiv abs/1804.

[10] Gorton GE, Hebert DA, Gannotti ME. Assessment of the kinematic variability among 12 motion analysis laboratories. Gait Post 2009;29:398–402. http://dx.doi.org/10.1016/j.gaitpost.2008.10.060

[11] Nigmatullin RR, Maione G, Lino P, Saponaro F, Zhang W. The general theory of the quasi-reproducible experiments: how to describe the measured data of complex systems? Commun Nonlin Sci Numer Simul 2017;42:324–41. http://dx.doi.org/10.1016/J.CNSNS.2016.05.019

[12] Nigmatullin RR, Zhang W, Yang R, Lu Y, Maione G. ''Universal'' fitting function for quantitative description of quasi-reproducible measurements. Comput Commun Collab 2017;5:8–34.

[13] Hak L, Houdijk H, van der Wurff P, Prins MR, Mert A, Beek PJ, et al. Stepping strategies used by post-stroke individuals to maintain margins of stability during walking. Clin Biomech 2013;28:1041–8. http://dx.doi.org/10.1016/J.CLINBIOMECH.2013.10.010

[14] Crane E, Gross M. Motion capture and emotion: affect detection in whole body movement. Affective computing and intelligent interaction. Berlin, Heidelberg: Springer; 2007. p. 95–101. http://dx.doi.org/10.1007/978-3-540-74889-2_9

[15] Kuzmych O, Awrejcewicz J, Aitouche A, Bahniuk N. Robust control for human postural balance: design and simulation. Proceedings of the 7th International Conference on Systems and Control; 2018. p. 454–61.

Please cite this article in press as: Nigmatullin RR, et al. Modeling and experimental validation of walking processes. Biocybern Biomed Eng (2019), https://doi.org/10.1016/j.bbe.2019.03.005